MDPI

Article

Experimental and Mechanistic Study of Synergistic Removal of Hg by Evaporation from Desulfurization Wastewater

Bin Hu [1,*]**, Cong Chen** [2] **, Yang Yi** [3]**, Shouxi Jiang** [1] **and Xiaosong Liu** [1]

[1] School of Physics and New Energy, Xuzhou University of Technology, Xuzhou 221018, China; 11922@xzit.edu.cn (S.J.); liuxiaosong@xzit.edu.cn (X.L.)
[2] Key Laboratory of Energy Thermal Conversion and Control of Ministry of Education, School of Energy and Environment, Southeast University, Nanjing 210096, China; chencong_china@seu.edu.cn
[3] State Key Laboratory of Natural and Biomimetic Drugs, School of Pharmaceutical Sciences, Peking University, Beijing 100191, China; yiyang@bjmu.edu.cn
* Correspondence: hubindndx@163.com

Abstract: The flue evaporation of desulfurization wastewater can solve the problem that it is difficult to remove some heavy metal ions and chloride ions by conventional methods. A large amount of chloride ions in desulfurization wastewater can also promote the catalytic oxidation removal of Hg in the flue gas. The migration character of chloride ions in the flue evaporation process of desulfurization wastewater was studied by using the coal-fired thermal state experimental platform. The concentrations of Hg^0 and Hg^{2+} in the flue gas at the inlet and outlet of selective catalytic reduction denitration (SCR), electrostatic precipitator (ESP), and wet desulfurization (WFGD) devices were tested, and the synergistic removal of traditional pollutant removal equipment by flue evaporation of desulfurization wastewater was analyzed. The influence of Hg and the effect of the evaporation of desulfurization wastewater at different positions on the removal of Hg in the flue gas were compared and analyzed, and the catalytic mechanism of Hg on the SCR surface was further revealed. The results show that 10% chloride ions enter the flue gas after the desulfurization wastewater evaporates. The content of chlorine elements and evaporation temperature influence the evaporation of desulfurization wastewater. The mechanism of SCR catalytic oxidation of Hg^0 was explored; oxygen atoms have catalytic oxidation effects on Hg^0 at different positions in the V_2O_5 molecule in SCR; and chloride ions can enhance the catalytic oxidation of Hg^0 by V_2O_5. The intermediate product HgCl is generated, which is finally converted into $HgCl_2$. The oxidation efficiency of Hg^0 in electrostatic precipitation (ESP) is increased from 3% to 18%, and the removal efficiency of Hg is increased from 5% to 10%. The removal efficiency of Hg^{2+} in WFGD is basically maintained at approximately 85%. In addition, a small amount of Hg^{2+} was restored to Hg^0 in WFGD. The removal efficiency of Hg^0 in the flue gas of evaporative desulfurization wastewater before SCR is 65%, and the removal efficiency of gaseous Hg is 62%. When the evaporative desulfurization wastewater before ESP, the synergistic removal efficiency of Hg^0 is 39%, and the gaseous Hg removal efficiency is 39%, and the removal efficiency of Hg is 40%. Evaporation of the desulfurization wastewater before SCR was more conducive to the coordinated removal of Hg by the device.

Keywords: evaporation of desulfurization wastewater; mercury; collaborative removal; catalytic oxidation

1. Introduction

At present, the limestone wet desulfurization process is commonly used in the removal of SO_2 pollutants in coal-fired power plants, which is mature, reliable in operation, and has high desulphurization efficiency [1–3]. During wet desulfurization, a large number of chlorides in the flue gas can be dissolved in the desulfurization slurry, which increases the concentration of chloride ions continuously. Ions, fluorides, heavy metal ions, and insoluble impurities are found in desulfurization wastewater [4–6]. The announcement of the Ministry of Environmental Protection's "Technical Policy for Pollution Prevention and Control

of Thermal Power Plants" clearly mentioned that the pollution caused by the discharge of wastewater from thermal power plants is to be prevented and that the implementation of zero-emission of desulfurization wastewater is encouraged [7]. At present, the evaporation of desulfurization wastewater is one of the technical means to achieve the "zero-emission" of desulfurization wastewater, which is also considered to be a potential and effective method for the treatment of desulfurization wastewater [8]. The evaporation process of desulfurization of wastewater droplets entering high temperature flue gas can be roughly divided into two stages. The first stage is similar to the free evaporation of water and the drying process of droplets in the second stage. When evaporation reaches equilibrium, solutes precipitate and exist as solid particulates [8]. At present, many studies have been carried out on the evaporation technology of desulfurization wastewater. Ran et al. [9] explored the low temperature flue gas environment from the perspective of theoretical analysis. Liang et al. [10] used thermogravimetric analysis (TGA) to study the effect of the heating rate and maximum temperature on the evaporation. Ma et al. [11] showed that the desulfurization wastewater evaporation realizes the cooling of flue gas and desulfurization wastewater zero discharge simultaneously. This work not only solves the cooling and desulfurization of coal-fired flue gas, but also effectively removes F^-, Cl^-, and heavy metal ions, which provides a new idea for the subsequent removal of mercury from coal-fired flue gas.

Mercury is a trace heavy metal contaminant that can permanently accumulate in organisms and the food chain, posing more significant threat to human health. Mercury in coal-fired flue gas exists in three forms: elemental mercury (Hg^0), oxidized mercury (Hg^{2+}), and particulate mercury (Hg^P). Hg^{2+} is easily soluble in water and easily captured by wet flue gas desulfurization systems; Hg^P exists in fly ash particles and can be removed by dust removal equipment [12–14], but Hg^0 is insoluble in water and difficult to adsorb, so Hg^0 has become a research focus in mercury pollution prevention and control. The removal of mercury includes two main methods: one is to use the adsorption of Hg^0 by the adsorbent, and the Hg^0 is fixed in the pores of the adsorbent to achieve the purpose of removal; the other is to use the catalytic oxidation of Hg^0 by the catalyst to convert Hg^{2+}. For the easily captured and water-soluble Hg^{2+} and Hg^P, they are removed together with fly ash in dust removal equipment or removed by scrubbing in a wet desulfurization system. The adsorbent method represented by activated carbon injection has limited its application in actual industry due to its high cost. Combined with a coal-fired flue gas electrostatic precipitator, wet flue gas desulfurization, and other existing pollutant control facilities (APCDs) to coordinate control of mercury emissions can meet the existing mercury emission standards and greatly reduce the cost of mercury removal. Therefore, it has also become an important research direction for mercury removal and management in coal-fired power plants [15–17]. Studies have shown that trace chlorine in coal is beneficial to the conversion of Hg^0 to Hg^{2+}. Chlorine can enhance the adsorption and fixation of mercury in coal-fired fly ash, while the content of chlorine in coal in China is generally low, limiting the amount of Hg^0 in flue gas [18,19]. Activated carbon injection is considered the best available and promising technology for controlling mercury emissions from coal-fired power plants [20]. However, the high cost of activated carbon makes this technology economically unfavorable [20]. Another method is adding sodium halide and ammonium halide. The additive method in coal increases the cost of mercury removal and easily causes equipment corrosion and "Secondary pollution" of the environment [18].

The chloride ion concentration can reach 20 g/L in desulfurization wastewater. During the evaporation process of the desulfurization wastewater in the limestone-gypsum wet desulfurization wastewater, the dissolved ions such as Ca^{2+}, Mg^{2+}, Na^+, Cl^-, and SO_4^{2-} rapidly crystallize and precipitate $CaCl_2$ and $NaCl$. Conventional chemical treatment of wastewater is a complex procedure. The solid product can promote the conversion of Hg^0 to Hg^{2+} and Hg^P in the flue gas to remove chloride ion. A novel treatment is proposed to evaporate desulfurization wastewater using waste heat in flue gas. This technology has been demonstrated in some power plants and realized wastewater zero discharge.

Chloride ion crystallizes on the fly ash surface in flue gas during evaporation process, which promoted the conversion of Hg^0 to Hg^{2+} and Hg^P in the flue gas [21,22].

With this novel technology, the APCDs may be enhanced and co-benefit Hg removal and oxidation efficiency. In this paper, the coal-fired thermal simulation experimental platform was used to experiment with the synergistic removal of Hg by the evaporation of desulfurization wastewater. Moreover, the effects of the wastewater evaporation position on Hg^0 oxidation and capture were investigated. In addition, based on the density functional theory (DFT), the catalytic oxidation mechanism of V_2O_5 for Hg was explored in SCR. The use waste heat to evaporate desulfurization wastewater can not only achieve zero discharge of desulfurization wastewater, but also enhance Hg removal efficiency. Finally, both theoretical and experimental results were thoroughly discussed, compared, and summarized, which will provide important reference for the industrial application.

2. Experimental Equipment and Theoretical Methods

2.1. Experimental Device

The coal-fired thermal state experimental system was built as shown in Figure 1. In this experimental system, coal-fired flue gas is generated by a coal-fired boiler, the flue gas flow is stabilized, and the flue gas temperature and the flue gas composition are adjusted in the buffer tank. The flue gas flows through the SCR reactor, there are three layers of honeycomb V_2O_5 catalyst, and the desulfurization wastewater evaporation nozzle is arranged above the catalyst. The evaporation chamber is arranged after the SCR, its diameter and height are 400 mm and 4000 mm respectively, and the upper part is also arranged with desulfurization wastewater evaporation nozzles. The electrostatic precipitator system consists of a wire-plate type electrode plate and a high-voltage power supply; a wet desulfurization system is arranged behind the precipitator, three-stage spraying is adopted, and a wire mesh demister is installed.
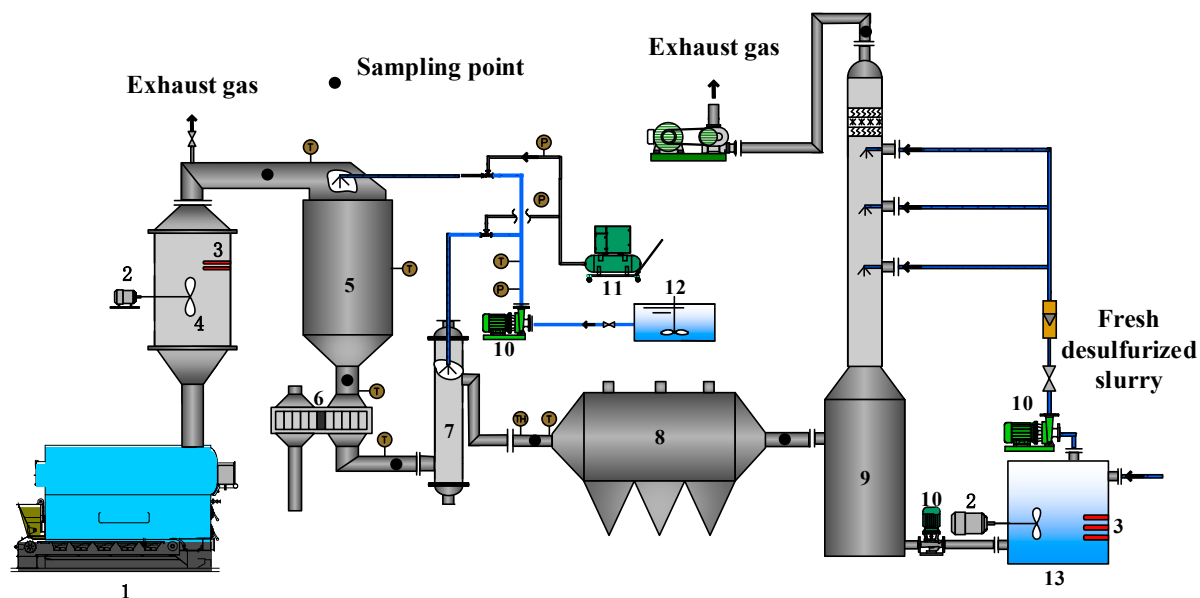

Figure 1. Coal-fired thermal state experimental system. 1—coal-fired boiler; 2—stirring rod; 3—heating rod; 4—buffer tank; 5—SCR; 6—heat exchanger; 7—evaporation chamber; 8—ESP; 9—WFGD; 10—water pump; 11—air compressor; 12—waste water tank; 13—slurry tank.

2.2. Test Methods

The mercury concentration is continuously detected online by a mercury analyzer (VM3000, Mercury Instruments, GmbH, Germany). This instrument has the advantages of rapid detection and accurate results, but VM3000 cannot directly measure the concentration of Hg^{2+} in flue gas. Therefore, a pretreatment device was designed as shown in Figure 2. In

this device, the flue gas passes through a freshly prepared 10% $SnCl_2$ solution, and Hg^{2+} is reduced to Hg^0. The acid gas in the flue gas is removed by a 1 mol/L KOH solution, and the total concentration of Hg is measured after drying. Using the same method, the flue gas is passed through 1 mol/L KCl solution and 1 mol/L KOH solution to remove Hg^{2+} and acid gas, the concentration of Hg^0 in the flue gas is measured after drying. The total concentration of Hg minus the Hg^0 concentration is the Hg^{2+} concentration.
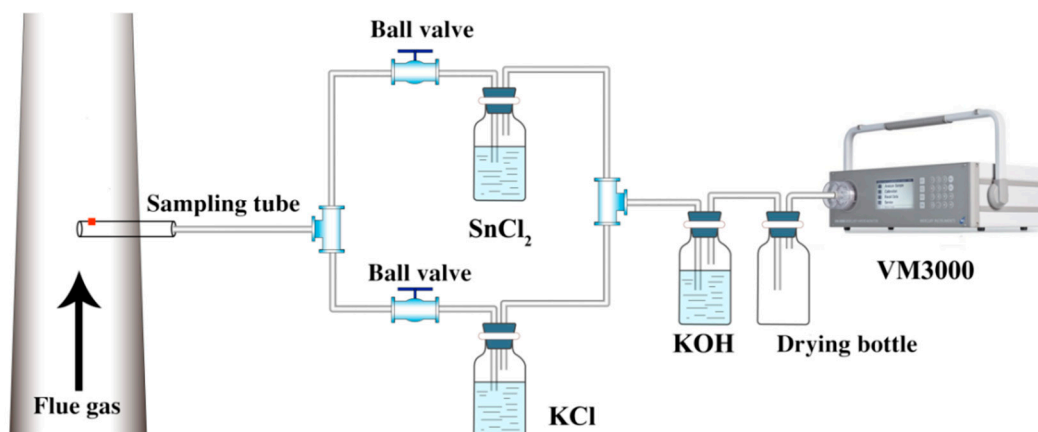

Figure 2. Hg sampling measurement device.

The oxidation (E_{oxi}) and removal (E_{cap}) efficiencies of Hg are defined as in Equations (1) and (2) [23,24]:

$$E_{oxi}(\%) = \frac{c(Hg_{in}^0) - c(Hg_{out}^0)}{c(Hg_{in}^0)} \times 100\% \qquad (1)$$

$$E_{cap}(\%) = \frac{c(Hg_{in}) - c(Hg_{out})}{c(Hg_{in})} \times 100\% \qquad (2)$$

In the formulas, the Hg^0 is the concentrations at the inlet and outlet of the device, respectively, $\mu g/m^3$; $c(Hg_{in}^0)$ and $c(Hg_{out}^0)$ are the total Hg concentrations in the inlet and outlet flue gas of the device, respectively, $\mu g/m^3$.

Gaseous chloride in flue gas was collected according to "Determination of Hydrogen Chloride in Ambient Air and Exhaust Gas-Ion Chromatography (HJ548-2016) [25]", using NaOH solution to collect samples and then using an ion chromatograph (ICS-2100) to test chloride ions in the absorption liquid.

2.3. Experimental Materials

The desulfurization wastewater is taken from the actual coal-fired power station, and the clarified liquid is obtained after precipitation and filtration. The corrosion and scaling characteristics, and the water quality analysis are shown in Table 1.

Table 1. Analysis of desulfurization wastewater quality.

Analyte Name	Concentration mg·L^{-1}	Analyte Name	Concentration mg·L^{-1}
Ca^{2+}	1204	Pb	0.52
Mg^{2+}	605	Cd	0.06
Cl^-	5049	Ni	0.27
F^-	12	Hg	0.12
NH_3/NH_4	500	Cu	0.11

The contents of the main components of the SCR catalyst are shown in Table 2. The catalyst is composed mainly of TiO_2, WO_3, SiO_2; TiO_2 is the carrier of the catalyst, V_2O_5

is the main active material, and WO_3 enhances the activity and thermal stability of the catalyst.

Table 2. XRF test results of the catalyst (wt.%).

Components	TiO$_2$	WO$_3$	SiO$_2$	SO$_3$	CaO	Al$_2$O$_3$
Content%	86.81	4.61	3.63	1.34	1.31	1.04
Components	**V$_2$O$_5$**	**Fe$_2$O$_3$**	**MgO**	**ZrO$_2$**	**Nb$_2$O$_5$**	
Content%	0.89	0.08	0.06	0.05	0.04	

2.4. Calculation Methods and Calculation Models

The density functional theory (DFT) calculation adopts the B3LYP calculation method of DFT for studying mercury adsorption process [26–28]. The mercury atom in the system is a heavy atom with 80 electrons, and a pseudopotential basis set for the effective core potential (ECP) must be used. The vibrational frequencies and thermodynamic properties of the computational model are based on the ideal gas approximation theory [29], the reaction energies are corrected with the basis set overlap error (BSSE) [30], and the calculation and analysis of bond order population numbers and natural bond orbitals (NBOs) reveal the intermolecular [31]. Gaussian09 software is used for all calculations; the B3LYP method is shown in Table 3; the calculated parameters with the experimental values under the two pseudopotential basis sets lanl2dz and lanl2mb were used and compared. Table 3 shows that the calculation results using the lanl2dz basis set are superior, lanl2dz is selected as the pseudopotential basis set of mercury in this paper.

Table 3. lanl2dz and lanl2mb comparison of the calculated and experimental values of the basis set.

Basis Group	lanl2dz	lanl2mb	Experimental Value [32]
HgCl	2.5744	2.6407	2.23
HgCl$_2$	2.4018	2.4176	1.84

3. Results and Discussion

3.1. Characteristics of Chloride Ion Precipitation in Desulfurization Wastewater

The temperature of the evaporation chamber was adjusted to 150–350 °C, and NaCl crystals were added to adjust the concentration of chloride ions in the desulfurization wastewater, and the evaporation amount was 15 L/h. The experimental results are shown in Figure 3. The temperature of the evaporation chamber increased from 150 °C to 350 °C. The concentration of chloride ions in the desulfurization wastewater was 10 g/L, and the mass fraction of chloride ions entering the gas phase increased from 8% to 12%, because the high temperature promoted the ionization of water to generate more H^+ and OH^-, so that Cl^- combined with H^+ to generate HCl. At high temperature, the HCl molecules volatilized into the gas phase, while the remaining Cl^- combined with metal cations; it precipitated in the form of crystalline salts and adhered to the surface of fly ash particles. With increase of temperature, the precipitated crystalline hydrate undergoes hydrolysis reaction at high temperature. The results showed that the concentration of chloride ions in the desulfurization wastewater and the evaporation temperature had effects on the evaporation of chlorine elements, but the effect was not significant.
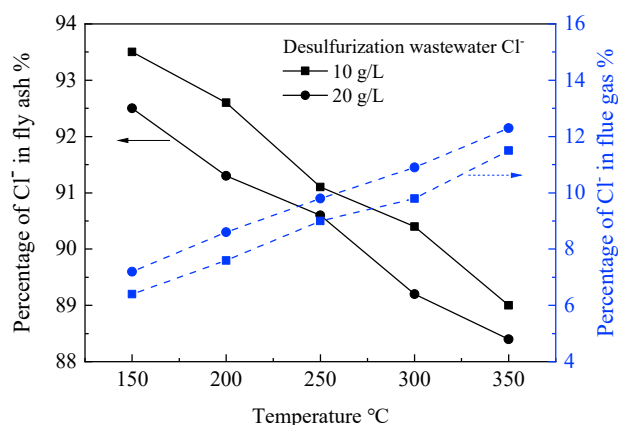
Figure 3. Evaporated Cl^- distribution of desulfurization wastewater with different Cl^- concentrations.

3.2. Mechanism of Enhanced SCR Oxidation of Hg^0 by Evaporation of Desulfurization Wastewater

The SCR catalyst can oxidize Hg^0 to Hg^{2+} and improve the removal effect of other equipment. The experiment investigated the effect of desulfurization wastewater evaporation on the SCR oxidation of Hg^0. The desulfurization wastewater evaporation volume was 15 L/h, the chloride ion mass concentration of desulfurization wastewater was adjusted to 10 g/L and 20 g/L, and the SCR temperature range was 200–400 °C. The oxidation efficiency of Hg^0 in the SCR device is as shown in Figure 4. The oxidation efficiency of Hg^0 was approximately 10% in the SCR catalyst. When the temperature increased, the oxidation efficiency increased slightly. When desulfurization wastewater evaporated before SCR, the oxidation efficiency of Hg^0 was significantly improved. Compared the evaporation of desulfurization wastewater with different chloride ion concentrations, the oxidation efficiency of Hg^0 increased with the increase of chloride ion concentration in the desulfurization wastewater. The results indicate that chloride ions were beneficial to promote the catalytic oxidation of Hg^0 by SCR.
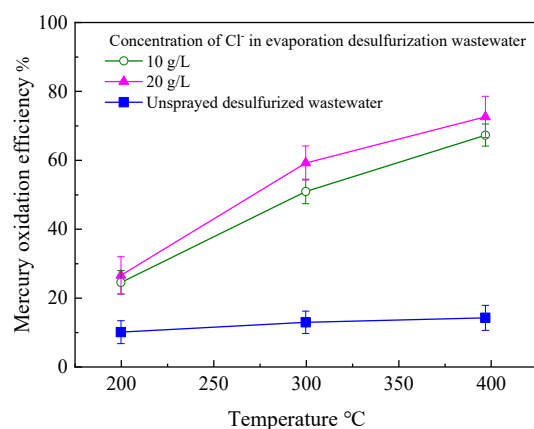

Figure 4. Oxidation efficiency of Hg^0 in the SCR device.

The oxidation efficiency of Hg^0 was higher at high temperature. With decreasing of temperature, the oxidation efficiency of Hg^0 gradually decreased [33,34]. When the desulfurization wastewater was evaporated, most of the chloride ions was adsorbed on the fly ash, and some of the chloride ions entered the gas phase. Chloride ions were deposited on the catalyst surface along with fly ash to form chloride ion active sites. Hg^0 flowed through the catalyst surface and reacted with chloride ion active sites, first generating unstable intermediate HgCl, and then forming stable $HgCl_2$ [33,34].

Temperature had an important impact on the oxidation of Hg^0 by SCR. It can be seen from Figure 4 that the oxidation efficiency of Hg^0 increased with the increasing temperature

mainly because the temperature affects the activity of the catalyst. There were few chloride ions, which was not conducive to the oxidation of Hg^0. In general, the flue gas temperature of the SCR device fluctuates in the range of 320–380 °C, the synergistic oxidation efficiency of Hg^0 can reach more than 60%.

Desulfurization wastewater evaporated before SCR, a large amount of chlorine entered into the flue gas to form active chloride ions (Cl^-), which promoted the catalytic oxidation of Hg^0 after passing through the SCR. The chlorine reaction mechanism of the ion-promoted V_2O_5 catalytic oxidation of Hg^0 was explored by DFT. The molecular structure of V_2O_5 is shown in Figure 5, and the oxygen atoms on the V_2O_5 molecule are defined as 0 and 1. The V_2O_5 molecule can catalyze the oxidation of Hg^0. The system containing V_2O_5 molecules and Hg atoms was established to calculate the energy change during the oxidation of Hg^0 by V_2O_5. The oxygen atoms at the 0 and 1 positions in the V_2O_5 molecule are shown in Figure 5. Since both of them can oxidize Hg^0, it is necessary to explore them separately.
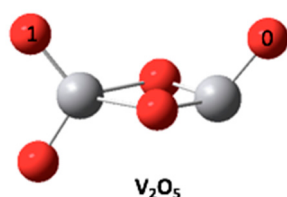

Figure 5. V_2O_5 molecular model.

The oxidation of Hg^0 by oxygen atoms at different positions on the 0 and 1 positions in the V_2O_5 molecule are shown in Figure 6. By analyzing the results, the bond distance between the oxygen at the 0 position and the Hg molecule was determined to be 2.983 Å, and the bond energy was 1.2 kcal/mol. However, the bond distance between the oxygen at the 1 position and the Hg molecule was 2.706 Å, and the bond energy was 2.29 kcal/mol. Therefore, the bond energy between Hg and O(1) was stronger. The Cl^- reacted with Hg^0 to generate HgCl and $HgCl_2$ in the flue gas, so it is necessary to further calculate the catalytic oxidation of HgCl on V_2O_5. The calculated results are shown in Figure 7. According to the proposed model, the bond distances formed by the reactions of O(0) and O(1) on HgCl and V_2O_5 were 2.210 Å and 2.181 Å, respectively. By calculating the bond energies for two different active sites, the bond energies are 43.03 kcal/mol and 61.03 kcal/mol, respectively. In addition, the reaction between $HgCl_2$ and O(1) on V_2O_5, the bond distance between them was 2.359 Å and the bond energy was 3.699 kcal/mol. The results indicated that there was a certain weak interaction between the two.
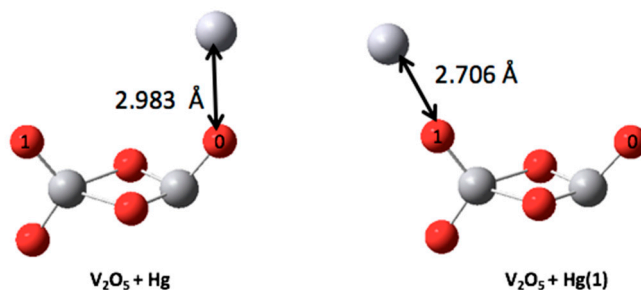

Figure 6. V_2O_5 and Hg reaction model.

The highest occupied molecular orbital (HOMO) binds its electrons more loosely and had electron donating properties, while the lowest unoccupied molecular orbital (LUMO) had a strong affinity for electrons and had electron accepting properties. These two orbitals were most likely to interact with each other and played an important role in chemical reactions. Therefore, it is necessary to explore the changes in the frontier orbitals during the oxidation of Hg^0. The HOMO and LUMO energies and frontier orbital calculations are

shown in Figure 8. The numerical results of the Hg^0 oxidation process natural bond orbital (NBO) charge transfer, HOMO, LUMO, and frontier orbitals are shown in Table 4.
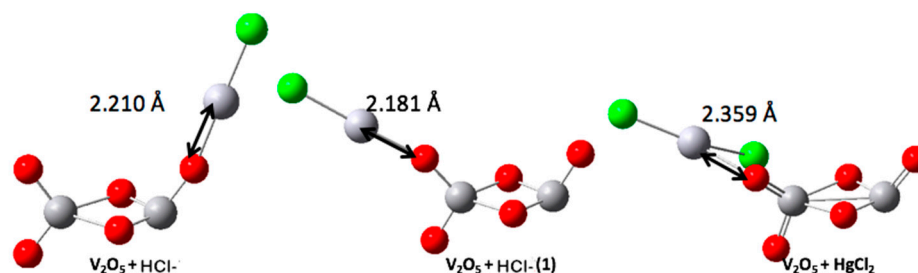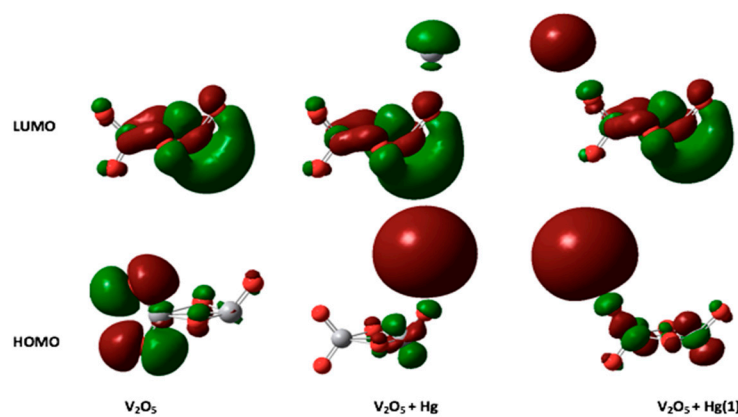

Figure 7. Reaction model of V_2O_5 and HgCl, $HgCl_2$.

Figure 8. Changes in HOMO and LUMO during Hg^0 oxidation.

Table 4. Calculation results of NBO charge transfer, HOMO), LUMO and frontier orbital during Hg^0 oxidation.

	Q_{NBO} (e)	E_{HOMO} (eV)	E_{LUMO} (eV)	E_g (eV)
V_2O_5	-	−8.657	−5.715	2.942
Hg	-	−6.483	−0.421	6.062
$HgCl^-$	-	−14.275	−11.714	2.562
$HgCl_2$	-	−8.539	−3.784	4.754
V_2O_5-Hg	0.142	−6.550	−5.500	1.050
V_2O_5-Hg (1)	0.210	−6.225	−5.466	0.760
V_2O_5-$HgCl^-$	−0.401	−12.548	−10.142	2.406
V_2O_5-$HgCl^-$ (1)	−0.425	−12.040	−9.829	2.211

In the reaction system of V_2O_5 and Hg, the charge transfer of O(0) and O(1) on V_2O_5 can be calculated as 0.142 eV and 0.210 eV, respectively. The charge transfer in the reaction system of V_2O_5 and HgCl was significantly higher than the charge transfer in the reaction system of V_2O_5 and Hg O(0) and O(1) charge transfer on V_2O_5, namely −0.401 eV and −0.425 eV, respectively. The charge transfer in the HgCl(1) reaction is significantly higher than the charge transfer in the V_2O_5-Hg(0) and V_2O_5-HgCl(0) reactions, which indicates that O(1) on the V_2O_5 molecule was the active site for catalyzed Hg oxidation. V_2O_5 can oxidize Hg^0, and Cl^- can enhance the oxidation and generate intermediate products (HgCl). When the reaction continues, it finally exists in the form of stable $HgCl_2$.

3.3. Desulfurization Wastewater Evaporation Enhanced Electrostatic Precipitation Removal of Hg

ESP can remove Hg^p in flue gas, but cannot remove Hg^{2+} in flue gas. The distribution of different forms of mercury in the electrostatic precipitator before and after the

evaporation of desulfurization wastewater is shown in Figure 9. The evaporation of desulfurization wastewater was 15 L/h, the mass concentration of chloride ions was 10 g/L, and the inlet flue gas temperatures of the SCR and electrostatic precipitator were 350 °C and 150 °C, respectively. The electrostatic precipitator voltage was −40 kV. The Hg^0 and Hg^{2+} concentrations in the flue gas at the SCR inlet were 40.12 μg/m^3 and 4.36 μg/m^3, respectively. The desulfurization wastewater was evaporated in the buffer tank before SCR and the evaporation chamber before the electrostatic precipitator. As shown in Figure 9, when the desulfurization wastewater was evaporated in the buffer tank before SCR, the ratio of Hg^0 and Hg^{2+} did not change before and after the electrostatic precipitator; the proportion increases from 30.6% to 48.5%. The active Cl^- formed by the evaporation of desulfurization wastewater can be adsorbed on the surface of fly ash to provide active sites for the oxidation of Hg^0. In addition, when the flue gas temperature decreases, part of the gaseous Hg will also be adsorbed on the surface of the fly ash, which will be removed by ESP.
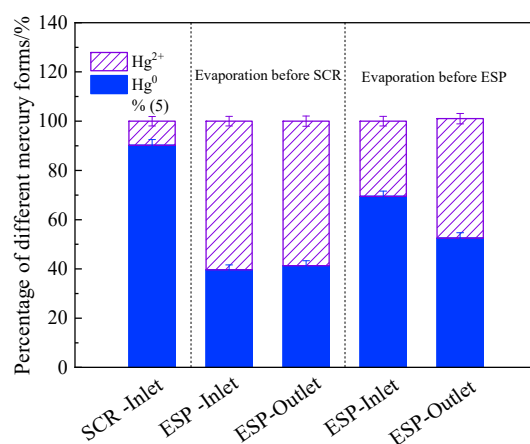

Figure 9. Influence of desulfurization wastewater evaporation on Hg speciation distribution in ESP.

Figure 10 shows the oxidation efficiency of Hg^0 and the removal efficiency of Hg in the electrostatic precipitator decreased slightly when the desulfurization wastewater is evaporated at different positions. The evaporation of desulfurization wastewater was 15 L/h, the mass concentration of chloride ions was 10 g/L, and the inlet flue gas temperatures of the SCR and electrostatic precipitator were 350 °C. The electrostatic precipitator voltage is −40 kV. The desulfurization wastewater was evaporated before SCR, the oxidation efficiency of Hg^0 in the ESP was increased from 2.6% to 6.4%, and the removal efficiency of Hg was increased from 5.1% to 10.6% showing that the evaporation of desulfurization wastewater can promote the oxidation of Hg^0, and at the same time, part of the Hg^0 was removed by ESP along with the fly ash.

3.4. Evaporation of Desulfurization Wastewater Enhanced WFGD for Hg Removal

The WFGD device can remove Hg^{2+} in the flue gas, but the device had little effect on the water-insoluble Hg^0. The effect of desulfurization wastewater evaporation on the simultaneously removal of Hg^{2+} by the WFGD system was studied experimentally. The desulfurization wastewater evaporation volume was 15 L/h, and the chloride ion concentration was 10 g/L. The liquid–gas ratio of the WFGD system was 15 L/m^3, which was the ratio of the total amount of circulating grout to flue gas. The desulfurization slurry temperature was 50 °C, the Hg^0 and Hg^{2+} concentrations of the SCR inlet flue gas were 40.12 μg/m^3 and 4.36 μg/m^3, respectively. The desulfurization wastewater was evaporated in the buffer tank and the evaporation chamber, respectively. The Hg^0 and Hg^{2+} concentrations at the inlet and outlet of the SCR, ESP, and WFGD units after the desulfurization wastewater were evaporated at different locations as shown in Table 5.
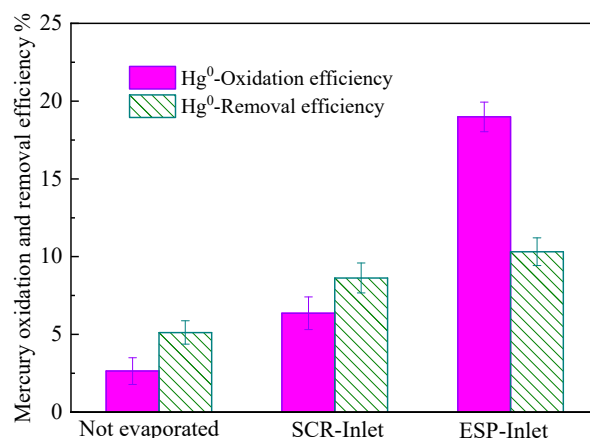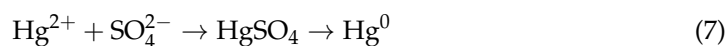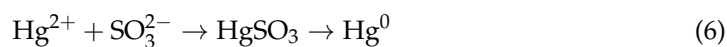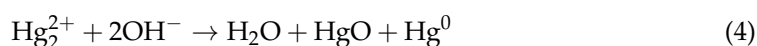
Figure 10. Effect of desulfurization wastewater evaporation on Hg removal by ESP.

Table 5. Concentrations of Hg^0 and Hg^{2+} at the inlet and outlet of different units of devices.

Evaporation Location	Mercury Form	Before SCR $\mu g \cdot m^{-3}$	After SCR $\mu g \cdot m^{-3}$	After ESP $\mu g \cdot m^{-3}$	After WFGD $\mu g \cdot m^{-3}$
Evaporation before SCR	Hg^0	40.12	15.96	12.42	14.23
	Hg^{2+}	4.36	24.32	17.63	2.26
Evaporation before ESP	Hg^0	40.12	27.63	20.98	24.63
	Hg^{2+}	4.36	13.25	12.16	1.65

　　　When the desulfurization wastewater was evaporated in the buffer tank, the Hg^{2+} concentration at the inlet and outlet of the WFGD unit decreases from 17.63 $\mu g/m^3$ to 2.26 $\mu g/m^3$, and the Hg^0 concentration increases from 12.42 $\mu g/m^3$ to 14.23 $\mu g/m^3$. The reasons being Hg^{2+} was soluble in water and dissolves in the desulfurization slurry in the WFGD device. At the same time, the Hg^0 concentration increased, and part of the Hg^{2+} in the flue gas was reduced to Hg^0. Numerous studies had found that Hg^{2+} in the WFGD device reduced to Hg^0. The current reaction mechanism is as follows (Equations (3)–(7) [35–37]):

$$Hg^{2+} + Hg^0 \rightarrow Hg_2^{2+} \tag{3}$$

$$Hg_2^{2+} + 2OH^- \rightarrow H_2O + HgO + Hg^0 \tag{4}$$

$$HgO + SO_2 \rightarrow Hg^0 + SO_3 \tag{5}$$

$$Hg^{2+} + SO_3^{2-} \rightarrow HgSO_3 \rightarrow Hg^0 \tag{6}$$

$$Hg^{2+} + SO_4^{2-} \rightarrow HgSO_4 \rightarrow Hg^0 \tag{7}$$

　　　Hg^{2+} and Hg^0 first react, and then combine with OH^- in the desulfurization slurry to form Hg^0 and HgO, and the generated HgO reacted with SO_2 in the flue gas to form Hg^0. In addition, the presence of numerous of reducing agents in the desulfurization slurry, such as various divalent metal ions, under the action of the reducing agent, Hg^{2+} generates $HgSO_3$ and $HgSO_4$. $HgSO_3$ and $HgSO_4$ decomposed to produce Hg^0 and released from the desulfurization slurry. The removal efficiency of Hg^0 and Hg^{2+} in the WFGD unit is shown in Figure 11. When the desulfurization wastewater was evaporated in the evaporation chamber, the removal efficiency of Hg^{2+} in the WFGD unit was 86.43%, and the release rate of Hg^0 was 17.42%. When the desulfurization wastewater was evaporated in the buffer tank, the removal efficiency of Hg^{2+} was 87.18%, and the release rate of Hg^0 was 14.57%. Comparing the efficiency of the WFGD unit for the simultaneously removal of Hg^{2+} from the evaporative desulfurization wastewater at different locations, the evaporation location of the desulfurization wastewater can be found to have little effect on the Hg^{2+} removal efficiency of the WFGD unit.
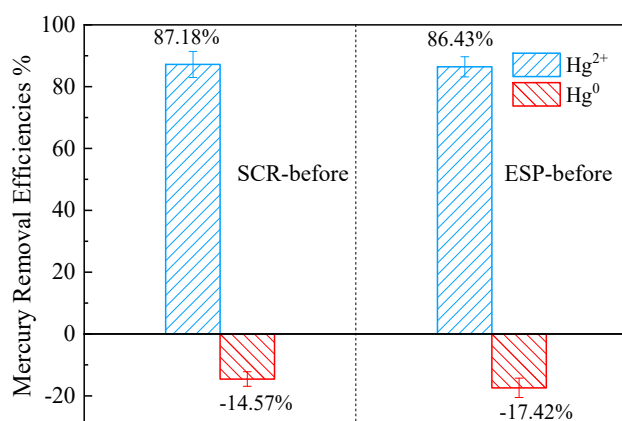
Figure 11. Removal efficiency of Hg^0 and Hg^{2+} in the WFGD device.

According to the results in Figure 12, it can be obtained that the evaporation of desulfurization wastewater at different positions changed the proportion of Hg^0 and Hg^{2+} in the flue gas. Therefore, evaporating desulfurization wastewater at different locations can ultimately affect the concentrations of Hg^0 and Hg^{2+} at the outlet of the WFGD unit. Figure 12 showed that the removal efficiency of Hg^0 and Hg^{2+} in the experimental device when the desulfurization wastewater was evaporated at different positions. When the desulfurization wastewater was evaporated before SCR, the simultaneous removal efficiency of Hg^0 was 64.53%, and the removal efficiency of Hg^{2+} was 68.16%. With desulfurization wastewater being evaporated before the ESP, the synergistic removal efficiency of Hg^0 was 38.61%, and the removal efficiency of Hg^{2+} was 40.19%. The evaporation of desulfurization wastewater before SCR was more conducive to the coordinated removal of Hg. The main reason was that the evaporation of desulfurization wastewater can significantly improve the oxidation of Hg^0 by the SCR catalyst, and most of the Hg^{2+} can be removed in the WFGD. Therefore, the proportion of Hg^{2+} increased, the synergistic removal efficiency of Hg can be improved.
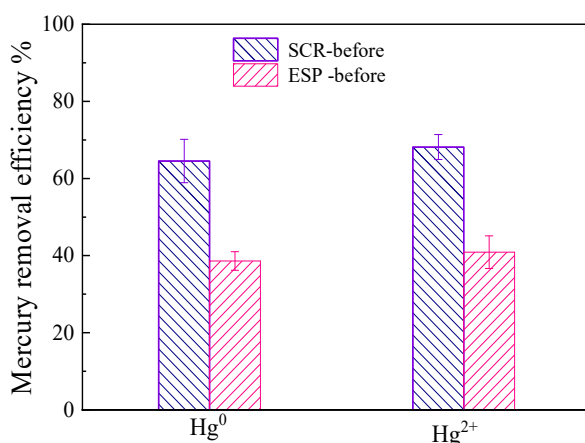

Figure 12. The effect of evaporative desulfurization wastewater at different positions on Hg removal efficiency.

4. Conclusions

This paper investigates the effect of the desulfurization wastewater on mercury removal from flue gas through a coal-fired thermal state experimental platform system. In this work, a coal-burning experimental device was built to investigate the mercury oxidation and removal during desulfurization wastewater evaporation process. The effect of the chloride ion in the desulfurization wastewater on the control of mercury emissions was explored. The migration and transformation behavior of mercury in the APCDs was system-

atically studied, and the mechanism of mercury removal from desulfurization wastewater was clarified.

Under typical working conditions, 10% chloride ions enter the flue gas with the desulfurization wastewater evaporation. When desulfurization wastewater evaporated before SCR, the oxidation efficiency of Hg0 was increased from 10% to 60%, and the flue gas temperature had an effect on the oxidation of Hg^0. The oxidation efficiency of Hg^0 in the electrostatic precipitator was increased from 2.6% to 6.4%, and the removal efficiency of Hg was increased from 5.1% to 10.6%. The removal efficiency of Hg^{2+} in the WFGD was more than 85% as well as a small amount of Hg^{2+} was reduced to Hg^0 by desulfurization slurry. In order to understand the mechanism of mercury oxidation efficiency across SCR deeply, theoretical investigations based on DFT calculations are required to explore the surface reactivity of V_2O_5 toward Hg. The catalytic oxidation of Hg0 by oxygen atom occurs at different positions of V_2O_5 molecule. The bond distance between O(0) and Hg atom was 2.983 Å, and the bond energy was 1.2 kcal/mol. The bond distance between O(1) and Hg atom was 2.706 Å, and the bond energy was 2.29 kcal/mol. Therefore, the oxidation between Hg and O(1) was strong. The bond distances formed by the reaction of O(0) and O(1) on HgCl and V_2O_5 were 2.210 Å and 2.181 Å, respectively, and the bond en-ergies were 43.03 kcal/mol and 61.03 kcal/mol, respectively. O(1) on V_2O_5 oxidizes with HgCl and HgCl was further oxidized to $HgCl_2$. V_2O_5 had a catalytic oxidation effect on Hg^0, and active chloride ions can enhance the oxidation effect, generate the intermediate product HgCl, and finally generate $HgCl_2$.

Finally, compared to the evaporation of desulfurization wastewater in different locations, when desulfurization wastewater was evaporated before SCR, the synergistic removal efficiency of Hg^0 was 64.5%, and the removal efficiency of Hg^{2+} was 62.2%. When the desulfurization wastewater was evaporated before the electrostatic precipitator, the synergistic removal efficiency of Hg^0 was 38.6%, and the removal efficiency of Hg^{2+} was 40.2%. Therefore, wastewater evaporation before SCR is beneficial to improve the oxidation and removal efficiency of mercury in APCDs. This technology realizes desulfurization wastewater zero discharge and simultaneously removal of Hg in flue gas.

Author Contributions: B.H.: writing—original draft, methodology, investigation, data curation. C.C.: writing—original draft, investigation. Y.Y.: DFT model building and simulation calculations. S.J.: investigation, project administration. X.L.: writing—review, editing, and funding acquisition. All authors have read and agreed to the published version of the manuscript.

Institutional Review Board Statement: Not applicable.

Informed Consent Statement: Not applicable.

Data Availability Statement: Not applicable.

Conflicts of Interest: The authors declare that they have no known competing financial interest or personal relationships that appeared to influence the work reported in this paper.

References

1. Tian, H.; Wan, D.; Che, Y.; Chang, J.; Zhao, J.; Hu, X.; Wang, L. Simultaneous magnesia regeneration and sulfur dioxide generation in magnesium-based flue gas desulfurization process. *J. Clean. Prod.* **2021**, *284*, 124720. [CrossRef]
2. Yan, X.; Xu, Y. SO_2 mitigation in China's coal-fired power plants: A satellite-based assessment on compliance and enforcement. *Atmos. Environ.* **2021**, *254*, 118396. [CrossRef]
3. Lee, J.; Cho, H.; Moon, I.; Lubomirsky, I.; Kaplan, V.; Kim, J.; Ahn, Y. Techno-economic assessment of carbonate melt flue gas desulfurization process. *Comput. Chem. Eng.* **2021**, *146*, 107227. [CrossRef]
4. Li, R.; Zhao, C.; Yang, W.; Ma, W.; Jia, Z.; Wang, C.; Cui, X.; Jiao, H. Experimental Study of Flue Gas Desulfurization Wastewater Zero Discharge from Coal-fired Power Plant. *AER-Adv. Eng. Res.* **2016**, *75*, 1000–1005.

5. Ma, S.; Chai, J.; Chen, G.; Wu, K.; Xiang, Y.; Wan, Z.; Zhang, J.; Zhu, H. Partitioning characteristic of chlorine ion in gas and solid phases in process of desulfurization wastewater evaporation: Model development and calculation. *Environ. Sci. Pollut. Res. Int.* **2019**, *26*, 8257–8265. [CrossRef]

6. Sun, Z.; Chen, H.; Zhao, N.; Feng, Y.; Liu, F.; Cai, C.; Che, G.; Yang, L. Experimental research and engineering application on the treatment of desulfurization wastewater from coal-fired power plants by spray evaporation. *J. Water Process Eng.* **2021**, *40*, 101960. [CrossRef]

7. *GB13223-2011*; Emission Standard of Air Pollutants for Thermal Power Plants. Ministry of Environmental Protection of the People's Republic of China, Standards Press of China: Beijing, China, 2015.

8. Zheng, C.; Zheng, H.; Yang, Z.; Liu, S.; Li, X.; Zhang, Y.; Weng, W.; Gao, X. Experimental study on the evaporation and chlorine migration of desulfurization wastewater in flue gas. *Environ. Sci. Pollut. Res.* **2019**, *26*, 4791–4800. [CrossRef]

9. Ran, J.; Zhang, Z. Numerical study on evaporation characteristics of different substance droplet in low temperature flue gas. *Proc. Csee* **2010**, *30*, 62–68.

10. Liang, Z.; Zhang, L.; Yang, Z.; Qiang, T.; Pu, G.; Ran, J. Evaporation and crystallization of a droplet of desulfurization wastewater from a coal-fired power plant. *Appl. Therm. Eng.* **2017**, *119*, 52–62. [CrossRef]

11. Shuangchen, M.; Jin, C.; Gongda, C.; Weijing, Y.; Sijie, Z. Research on desulfurization wastewater evaporation: Present and future perspectives. *Renew. Sustain. Energy Rev.* **2016**, *58*, 1143–1151. [CrossRef]

12. Chen, C.; Duan, Y.; Zhao, S.; Hu, B.; Li, N.; Yao, T.; Zhao, Y.; Wei, H.; Ren, S. Experimental study on mercury removal and regeneration of SO_2 modified activated carbon. *Ind. Eng. Chem. Res.* **2019**, *58*, 13190–13197. [CrossRef]

13. Yang, Y.; Liu, J.; Ding, J.; Yu, Y.; Zhang, J. Mercury/oxygen reaction mechanism over $CuFe_2O_4$ catalyst. *J. Hazard. Mater.* **2021**, *424*, 127556. [CrossRef] [PubMed]

14. Zhou, Q.; Di, Y.; Tao, X.; Song, T.; Lu, P.; Xu, G.; Dong, L. Influence of Mo doping on mercury capture and SO_2 tolerance of $Mo_xFe_6Mn_{1-x}O_y$ magnetic sorbent. *Fuel* **2022**, *38*, 121980. [CrossRef]

15. Liu, Z.; Liu, D.; Zhao, B.; Feng, L.; Ni, M.; Jin, J. Mercury removal based on adsorption and oxidation by fly ash: A review. *Energy Fuels* **2020**, *34*, 11840–11866. [CrossRef]

16. Wang, H.; Duan, Y.; Ying, Z.; Xue, Y. Studies on mercury adsorption species and desorption activation energy on activated carbon under oxy combustion. *Energy Fuels* **2018**, *32*, 193–200. [CrossRef]

17. Li, Y.; Chen, M.; Xue, Z.; Zhi, G.; Ma, J.; Liu, Y.; Gao, W. Research on synergistic mercury removal of coal-fired power plants. *Chem. Ind. Eng. Prog.* **2014**, *33*, 2187–2191.

18. Yang, Y.; Liu, J.; Liu, F.; Wang, Z.; Ding, J. Comprehensive Hg/Br reaction chemistry over Fe_2O_3 surface during coal combustion. *Combust. Flame* **2018**, *196*, 210–222.

19. Wu, S.; Ozaki, M.; Sasoka, E. Development of iron-based sorbents for Hg^0 removal from coal derived fuel gas: Effect of hydrogen chloride. *Fuel* **2008**, *87*, 467–474. [CrossRef]

20. She, M.; Duan, Y.; Zhu, C.; Jia, C.Q. Impact of nonoxidized sulfur species on elemental mercury removal by SO_2 activated petroleum cokes. *Energy Fuels* **2020**, *34*, 14388–14399. [CrossRef]

21. Xu, Y.; Jin, B.; Zhou, Z.; Fang, W. Experimental and numerical investigations of desulfurization wastewater evaporation in a lab-scale flue gas duct: Evaporation and HCl release characteristics. *Environ. Technol.* **2021**, *42*, 1411–1427. [CrossRef]

22. Bin, H.; Yang, Y.; Cai, L.; Yang, L.; Roszak, S. Enhancing mercury removal across air pollution control devices for coal-fired power plants by desulfurization wastewater evaporation. *Environ. Technol.* **2017**, *40*, 154–162. [CrossRef] [PubMed]

23. Zhao, S.; Xu, H.; Mei, J.; Ma, Y.; Lou, T.; Qu, Z.; Yan, N. Ag-Mo modified SCR catalyst for a co-beneficial oxidation of elemental mercury at wide temperature range. *Fuel* **2017**, *200*, 236–243. [CrossRef]

24. Chen, C.; Jia, W.; Liu, S.; Cao, Y.; Zhao, B.; Wang, J. Catalytic performance of $CuCl_2$-modified V_2O_5-WO_3/TiO_2 catalyst for Hg^0 oxidation in simulated flue gas. *Korean J. Chem. Eng.* **2018**, *35*, 637–644. [CrossRef]

25. Ministry of Ecology and Environment of the People's Republic of China. *Determination of Hydrogen Chloride in Ambient Air and Exhaust Gas-Ion Chromatography*; Ministry of Ecology and Environment of the People's Republic of China: Beijing, China, 2016.

26. Lee, C.; Yang, W.; Parr, R.G. Development of the Colle-Salvetti correlation-energy formula into a functional of the electron density. *Phys. Rev. B Condens. Matter* **1988**, *37*, 785. [CrossRef] [PubMed]

27. Tian, L.; Chen, F. Multiwfn: A multifunctional wavefunction analyzer. *J. Comput. Chem.* **2012**, *33*, 580–592.

28. Becke, A.D. Density-functional thermochemistry. *J. Chem. Phys.* **1993**, *98*, 5648. [CrossRef]

29. Miehlich, B.; Savin, A.; Stoll, H.; Preuss, H. Results obtained with the correlation energy density functionals of becke and Lee, Yang and Parr. *Chem. Phys. Lett.* **1989**, *157*, 200–206. [CrossRef]

30. Davidson, N. *Statistical Mechanics (McGraw Hill Series in Advanced Chemistry)*; Courier Corporation: New York, MA, USA, 1962.

31. Reed, A.E.; Curtiss, L.A.; Weinhold, F. Intermolecular interactions from a natural bond orbital, donor-acceptor viewpoint. *Chem. Rev.* **1988**, *88*, 899–926. [CrossRef]

32. Liu, J.; Qu, W.; Yuan, J.; Wang, S.; Qiu, J.; Zheng, C. Theoretical Studies of Properties and Reactions Involving Mercury Species Present in Combustion Flue Gases. *Energy Fuels* **2010**, *24*, 509–518. [CrossRef]

33. Zhang, J.; Duan, Y.; Zhao, W.; Zhu, C.; Zhou, Q.; Ding, W. Study on Elemental Mercury Oxidation by Non-thermal Plasma with Calcium Chloride Enhancement. *Plasma Chem. Plasma Processing* **2018**, *38*, 573–586. [CrossRef]

34. Liu, J.; He, M.; Zheng, C.; Chang, M. Density functional theory study of mercury adsorption on V_2O_5(001) surface with implications for oxidation. *Proc. Combust. Inst.* **2011**, *33*, 2771–2777. [CrossRef]

35. Zhao, S.; Pudasainee, D.; Duan, Y.; Gupta, R.; Liu, M.; Lu, J. A review on mercury in coal combustion process: Content and occurrence forms in coal, transformation, sampling methods, emission and control technologies. *Prog. Energy Combust. Sci.* **2019**, *73*, 26–64. [CrossRef]

36. Zhu, C.; Duan, Y.; Wu, C.Y.; Zhou, Q.; She, M.; Yao, T.; Zhang, J. Mercury removal and synergistic capture of SO_2/NO by ammonium halides modified rice husk char. *Fuel* **2016**, *172*, 160–169. [CrossRef]

37. Jiang, Y.Z.; Chen, C.M.; Jiang, L.X.; Liu, S.T.; Wang, B. Study of mercury re-emission from simulated wet flue gas desulfurization liquors. *Adv. Mater. Res.* **2013**, *610*, 2033–2037.